AAS 10-055

ORION OPTICAL NAVIGATION FOR LOSS OF COMMUNICATION LUNAR RETURN CONTINGENCIES

Joel Getchius
Jacobs Engineering

Chad Hanak
NASA Johnson Space Center

Daniel G. Kubitschek
Lockheed Martin Space Systems Company

33rd ANNUAL AAS GUIDANCE AND CONTROL CONFERENCE

February 6 - February 10, 2010
Breckenridge, Colorado

Sponsored by
Rocky Mountain Section

AAS Publications Office, P.O. Box 28130 - San Diego, California 92198

ORION OPTICAL NAVIGATION FOR LOSS OF COMMUNICATION LUNAR RETURN CONTINGENCIES

Joel Getchius, Chad Hanak and Daniel G. Kubitschek

The Orion Crew Exploration Vehicle (CEV) will replace the Space Shuttle and serve as the next-generation spaceship to carry humans back to the Moon for the first time since the Apollo program. For nominal lunar mission operations, the Mission Control Navigation team will utilize radiometric measurements to determine the position and velocity of Orion and uplink state information to support Lunar return. However, in the loss of communications contingency return scenario, Orion must safely return the crew to the Earth's surface. The navigation design solution for this loss of communications scenario is optical navigation consisting of lunar landmark tracking in low lunar orbit and star- horizon angular measurements coupled with apparent planetary diameter for Earth return trajectories. This paper describes the optical measurement errors and the navigation filter that will process those measurements to support navigation for safe crew return.

INTRODUCTION

Previous work has examined the feasibility, sensitivity, and performance of the concept of Orion optical navigation.[4, 6] Optical navigation is the backup form of navigation for lunar missions in the case of loss of communications with the ground. For a nominal Earth return, the navigation performance must be sufficient to support the execution of a three-burn trans-Earth Injection (TEI) sequence that places Orion on a return trajectory to Earth. Furthermore, the optical navigation performance must be sufficient to ensure a safe re-entry for the crew. Additionally, three Trajectory Correction Maneuvers (TCMs) are scheduled to remove targeting and maneuver execution errors and ensure that the appropriate entry interface conditions are met to achieve a safe entry corridor within the capability of the thermal protection system and crew load limits. Figure 1 illustrates the Earth return trajectory profile.

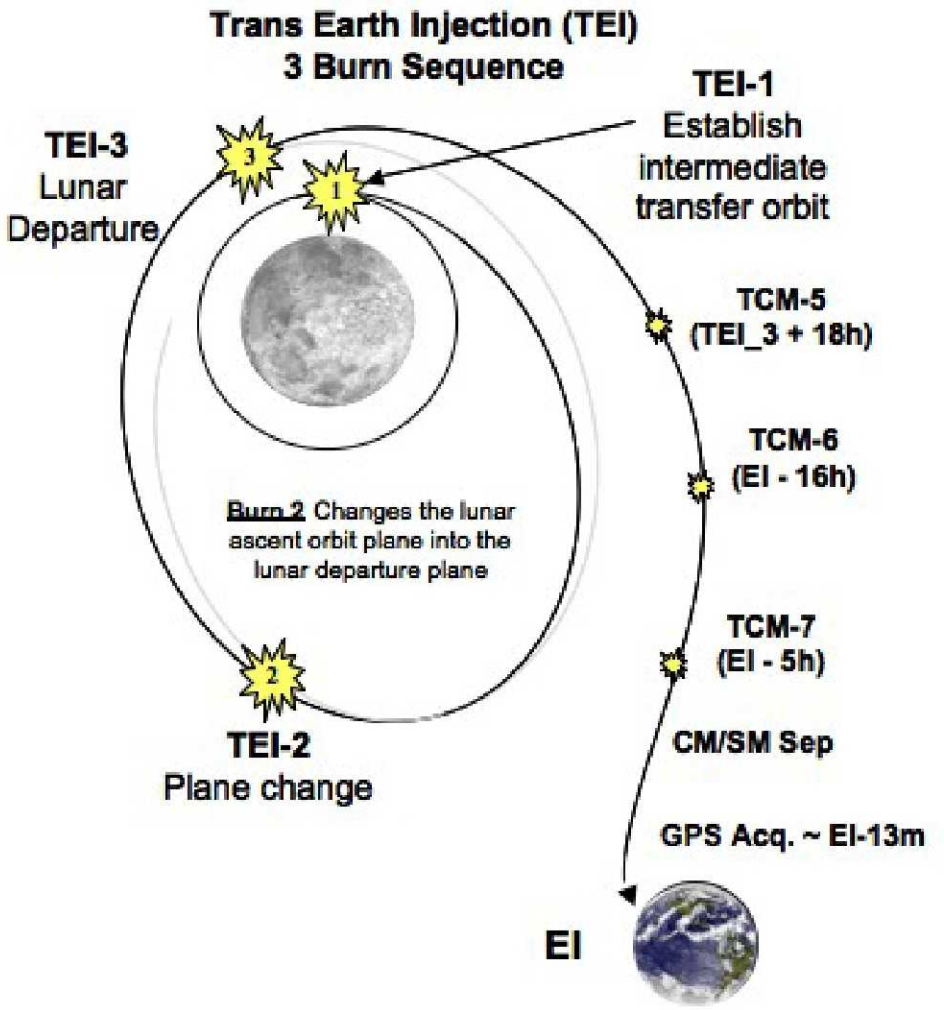

Figure 1: Orion Earth Return From Moon Trajectory Profile.

While loss of communication can occur anytime during the mission, Orion is only responsible for safe return following successful Lunar orbit insertion (LOI). Therefore, the optical navigation performance must support both TEI and TCM targeting such that the Δv dispersions and entry interface conditions are within the capabilities of the system. To protect for the loss of communications following LOI, the nominal concept of operations includes acquisition and processing of optical navigation images and estimation of the independent optical navigation state in parallel with the ground-based radiometric navigation process to monitor quality. In the event of a loss of communication, the optical navigation state will become the primary navigation state used for Earth return.

Two different types of optical navigation measurments are available for Orion, depending on whether the vehicle is in low lunar orbit or cis-lunar space. These include the use of

the angle formed by a star and Earth or Moon horizon and the apparent angular diameter of either the Earth or Moon as the measurements for cis-lunar space (region during transit to/from the Moon) and the angular location of lunar landmarks (i.e. craters) as measurements in low lunar orbit (LLO). We refer to the former as "Celestial Navigation" and the later as "Lunar Landmark Tracking." Figure 2 and illustrates these measurements.

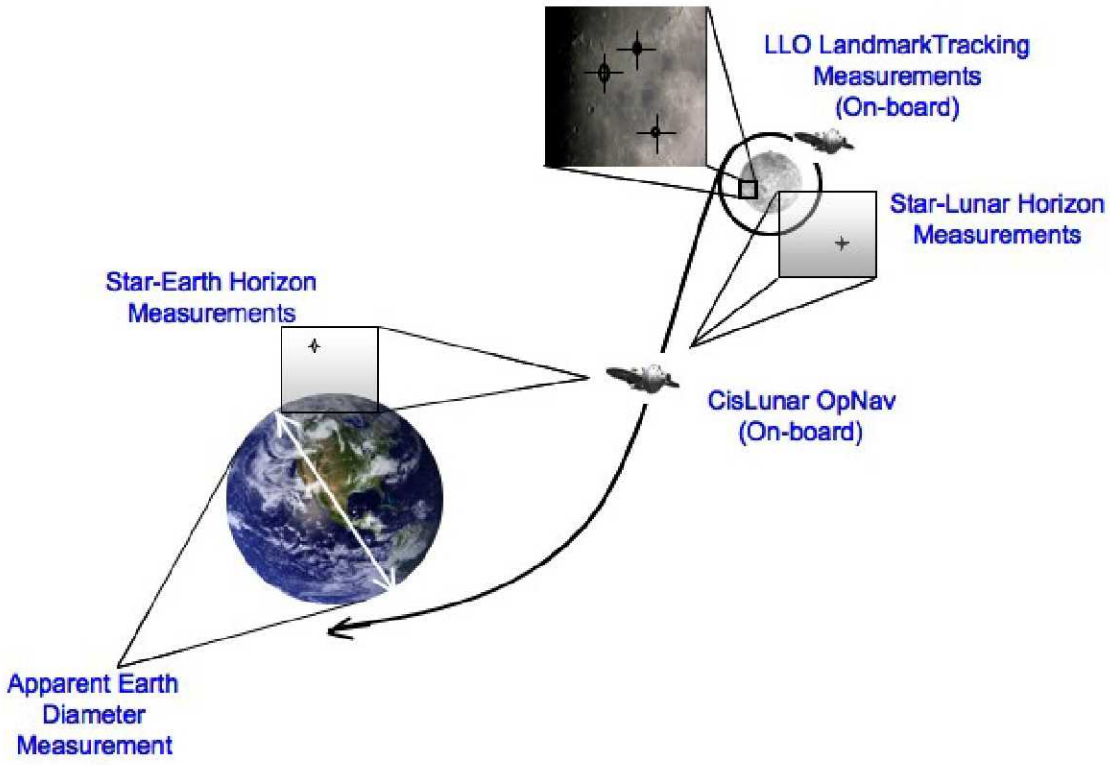

Figure 2: Optical Navigation Measurements.

Tables 1 and 2 show the contributing error sources for Celestial Navigation and Lunar Landmark Tracking measurements, respectively. Measurement error allocations are established and based on the bounding optical navigation performance needed to meet the Δv dispersions and entry interface conditions.

Table 1: Celestial Navigation measurement errors.

Measurement	Error Source
Star Centroiding	Camera pixel resolution
	Camera point-spread-function (PSF)
	Geometric distortion
	Background level
	Read noise
	Shot noise

Stellar Subpoint Location	Camera pixel resolution
	Camera PSF
	Atmospheric variation (Earth)
	Topographic variation (Moon)
	Background level
	Geometric distortion
	Read noise
	Shot noise
	Camera pixel resolution
	Camera PSF
	Atmospheric variation (Earth)
	Topographic variation (Moon)
	Background level
	Geometric distortion
	Read noise
	Shot noise

Table 2: Lunar Lankmark Tracking measurement errors.

Measurement	**Error Source**
Landmark Bearing	Camera pixel resolution
	Camera point-spread-function (PSF)
	Camera attitude knowledge error
	Landmark catalog location error
	Background level
	Geometric distortion
	Read noise
	Shot noise

Celestial Navigation and Lunar Landmark Tracking measurements will be computed using image processing algorithms running on the Vision Processing Unit (VPU). The VPU is a standalone computer tasked with the image processing and image data handling functions on the Orion vehicle. Once the measurements have been generated, they are passed to the Orion Vehicle Management Computer (VMC) where the navigation filters reside.

This paper describes the navigation state parameterization and candidate filtering algorithms used for optical navigation. The results presented in this paper used the Matlab based Spacecraft Tracking and Data Network (a three degree-of-freedom simulation initially designed for radiometric tracking analysis) augmented to support the processing of optical navigation measurements.

DYNAMICAL MODELS[5]

The STDN simulation maintains two vehicle states: an environment, or "truth" state, and a navigation or filter state. Initially, the environment state is randomly perturbed based on the initial environment dispersion covariance assigned. This perturbation is calculated via a Gaussian random number generator and the square root of the covariance diagonals. The initial environment covariance was based on a 150 m one-sigma position uncertainty and a 0.3 m/s one-sigma velocity uncertainty in each inertial J2000 axis (spherical covariance). The state perturbation was performed in inertial coordinates and no correlations are assigned. These values were chosen by engineering judgmentand consultation with Apollo era engineers.

The navigation state is the initial environment state perturbed via a dispersion covariance. This dispersion covariance was based on a 5 km one-sigma position uncertainty and a 5 m/s one-sigma velocity uncertainty in each inertial axis. The off-diagonal elements were initialized to zero. Once again, these values were chosen by engineering judgment.

Both the navigation and environment states are propagated with a fixed step Encke-Nystrom integrator. Perturbations include gravitational accelerations from the Sun, Earth, Moon, and as well as non-spherical gravity terms of the primary body (in this case, the Moon). For the navigation state, a 4 x 4 LP150Q lunar gravity field was utilized which is in contrast to the environment where a dispersed 30 x 30 LP150Q lunar gravity model was utilized. The truncation of the navigation gravity field was done so in order to reflect the current Orion absolute navigation design for the propagation of states. The dispersed gravity model was formulated by randomly dispersing the non-spherical gravity terms with their associated uncertainties at simulation initialization. Finally, a perturbation to account for the vehicle acceleration from thruster firings and venting is also included in the equations of motion. For the environment state, this is modeled as an additional acceleration term with a Gauss-Markov formulation. The associated time constant and 1-sigma value is approximately 12 hrs and 2 μg's respectively for each UVW axis. UVW is a spacecraft centered coordinate frame where U points to the center of the planetary body, W is along the angular moment vector, and V is orthogonal to U and W. For the navigation state, the unmodeled accelerations are solved for by the filter and utilized in the state integration.

MEASUREMENT MODELS

Lunar Landmark Tracking Measurement Models

The Lunar landmark bearing measurement allocation of 0.07 deg (3σ) has been assumed for this analysis. The ability to locate the landmark (crater) in the image is taken to be approximately 0.05 times the radius of the landmark[6,7] (the larger the landmark diameter, the larger the bearing error), then the landmark catalog must be limited to landmarks of

0.07/0.05 deg or 1.4 deg or less. For a 100 km altitude orbit, the maximum landmark diameter would be 4.9 km. Figure 3 shows the availability of Lunar landmarks of diameter 5 km or less within a 20 deg field-of-view (FOV) at an altitude of 100 km. A 20 deg FOV is representative of a typical wide angle camera (WAC) used in spaceflight applications. Assessment of the error sources listed in table 2 will define the camera characteristics needed to support Lunar Landmark Tracking measurements.

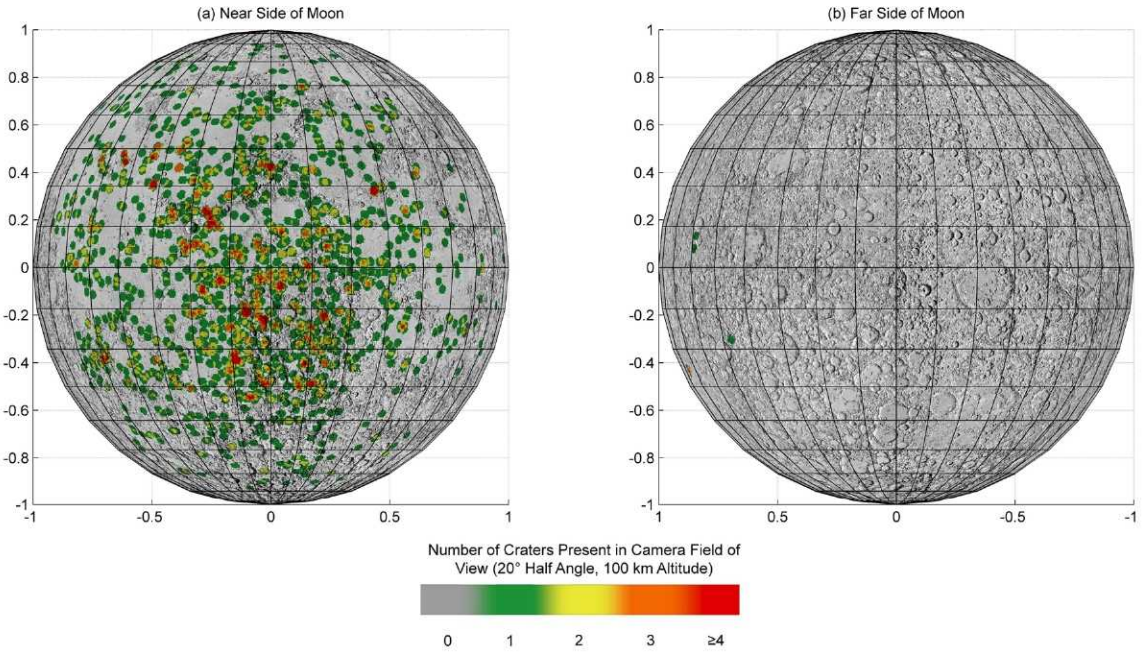

Figure 3: Sample lunar landmark tracking measurement availability.

Celestial Navigation Measurement Models

As previously mentioned, celestial navigation measurement quality allocations have been established. Table 3 describes the measurement errors that may be expected for celestial navigation and which were assumed for this analysis.

Table 3: Celestial Navigation measurement quality.

Parameter	3σ Value
Star centroiding noise	15 arc-seconds
Star centroiding bias	10 arc-seconds
Stellar subpoint location noise	15 arc-seconds
Stellar subpointlocation bias	6 arc-seconds
Apparent planetary diameter noise	9 km
Apparent planetary diameter bias	9 km

Note that the apparent planetary diameter is not specified as an angle. This is due to the expected impact of either the lunar terrain or the Earth's atmosphere on the ability to resolve the horizon. Therefore, these noise and bias terms will feed into the resultant bias and noise for the celestial navigation measurements, and the magnitude of this impact will be range dependent.

A cursory look at the star field (Figure 3) considering stars with a magnitude of 5 and brighter reveals a fairly isentropic distribution.[1] Therefore, one may conclude that the availability or measurements (and therefore the navigation performance of celestial navigation) is fairly independent of trajectory.

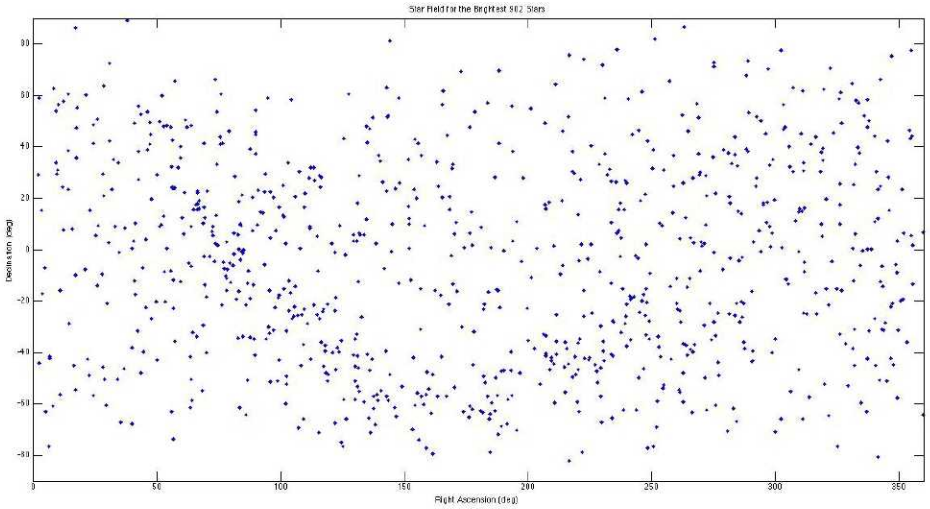

Figure 4: Star field for magnitude 5 and brighter.

For a typical 3.5 day return trajectory, the number of measurements available can be seen in Figure 4.

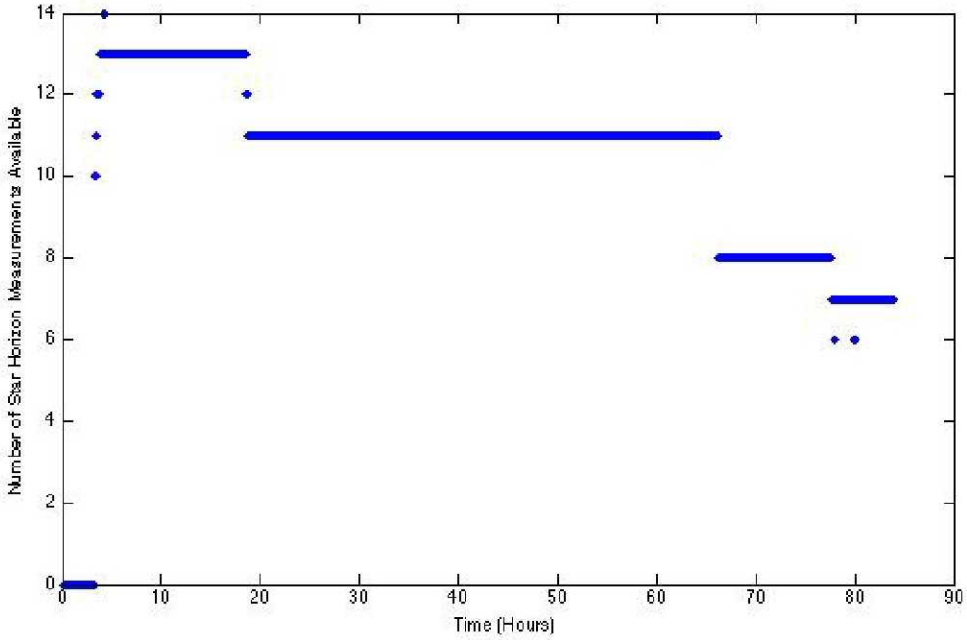

Figure 5: Number of celestial navigation measurements available.

Due to attitude constraints driven by thermal and power considerations, Orion will nominally be oriented in a tail-to-sun attitude during Earth return which may require reorientation to point the cameras for celestial navigation imaging. Therefore, a celestial navigation "tracking pass" schedule has been assumed with the following considerations:

1. Passes are one hour in length.
2. One pass occurs prior to each TCM execution to ensure a quality navigation state for maneuver targeting operations.
3. If maneuvers are not executed for an extended period of time, additional passes are performed to maintain the navigation state.

Based on these considerations, a sample measurement tracking schedule can be constructed (Figure 4).

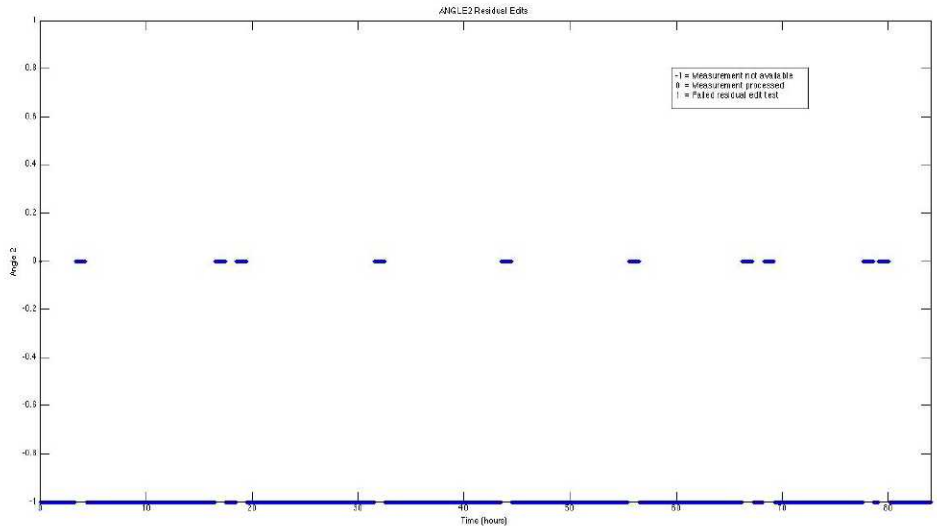

Figure 6: Sample celestial navigation tracking schedule.

FILTER DESIGN

Three mechanizations of navigation filters were studied in this paper: a linearized Kalman filter, an Extended Kalman filter, and a batch sequential filter.

Linearized Kalman Filter

The linearized Kalman filter (or error state filter) utilizes a scalar state update algorithm to solve for an error state that is propagated via the state transition matrix. After every hour of processing, the reference state was "rectified" with the filter error state from the reference state. The covariance update equation has been augmented to account for suboptimal filter design. Additionally, the calculation of the Kalman gain included a decaying "underweighting factor" that has the impact of reducing the impact of initial transients on filter performance. The covariance was propagated in time via the state transition matrix, which was calculated by integrating the time derivative of the state transition matrix via the linear variance equation. The following equations represent the mechanization of the linearized Kalman filter[3].

In order to model a "lost in space" initial navigation knowledge, the knowledge covariance was initialized with a 100 km, 1-sigma, in each position axis and 10 m/s, 1-sigma in each velocity axis. These specific numbers were chosen by engineering judgment.

Extended Kalman Filter

The mechanization of the extended Kalman filter is exactly that of the linearized Kalman

filter except the rectification of the reference state with occurring at every integration time step.

Least Squares Sequential Batch Filter

Finally, a sequential least squares batch filter was also utilized. This algorithm is configurable to utilize a priori covariance information or none at all. No additional algorithm enhancements were made to the batch filter. The batch filter is deemed to be converged when the pre and post fit RMS residuals differ by less than 1%. The number of iterations is capped at 10, if convergence is not obtained in 10 iterations, the batch is discarded without updating the navigation state.

Filter State Parameterization Options

Three state parameterization options were examined. Table 1 lists each option.

Table 2: Filter state parameterization options.

Option	States
PRM-1	Orion inertial position and velocity states.
PRM-2	PRM-1 state parameterization and measurement angle biases.
PRM-3	PRM-2 state parameterization and unmodeled acceleration states.

Note that when option PRM-1 was utilized, the uncertainty measurement weighting in the filter algorithms was increased by a factor of $\sqrt{2}$. This was done because as the bias terms were not solved for the effective measurement uncertainty increased. PRM-2 solves for one bias state for type of measurement (apparent planetary diameter, lunar landmark bearing, or star-horizon). PRM-3 solves for unmodeled accelerations that subsequently utilized in the navigation state propagation.

NAVIGATION PERFORMANCE

Linearized Kalman Filter Performance for Celestial Navigation

First, a study utilizing a 3.5 day Earth return trajectory was conducted to examine the performance of this sequential filter mechanization and trade the appropriate state parameterization. Figure 7 illustrates the navigation errors for the linearized Kalman filter algorithm.

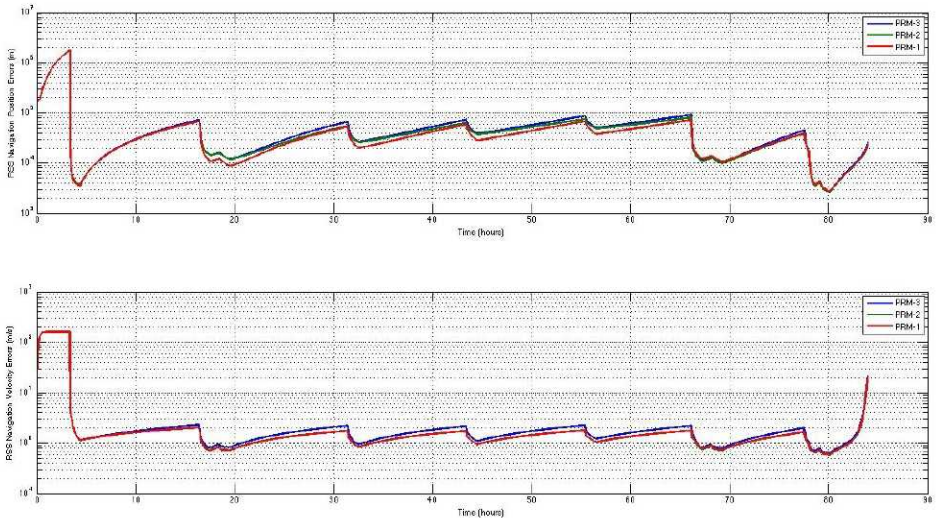

Figure 7: Linearized Kalman filter navigation errors for celestial navigation and a variety of state parameterization options.

Note that while similar in performance, state parameterization option PRM-1 slightly outperforms the other two options. Most likely, this is due to several factors:

1. The relative weakness of the optical navigation measurements, and therefore the inability to accurately solve for the measurement bias states.
2. The short period of measurement tracking and weak dynamics in cis-lunar space making solving for the unmodeled acceleration states difficult.
3. The mechanization of a single bias term as applicable to every star-horizon measurement instead of solving for a bias for each star-horizon measurement.

Items 1 and 2 are difficult to overcome. Item 3 may prove in the future to aid in the performance of celestial navigation, however it will drastically increase the complexity of the software. Bias states would have to be solved for each star, and maintained – potentially increasing the number of filter states to over 900. Having such a large state parameterization may prove unwieldy, especially if the improvement of the navigation performance is only slight.

Extended Kalman Filter Performance for Celestial Navigation

Next, the extended Kalman filter mechanization was examined for all three state parameterization options and compared to the results of the linearized Kalman filter. Figure 8 illustrates the navigation performance of the extended Kalman filter.

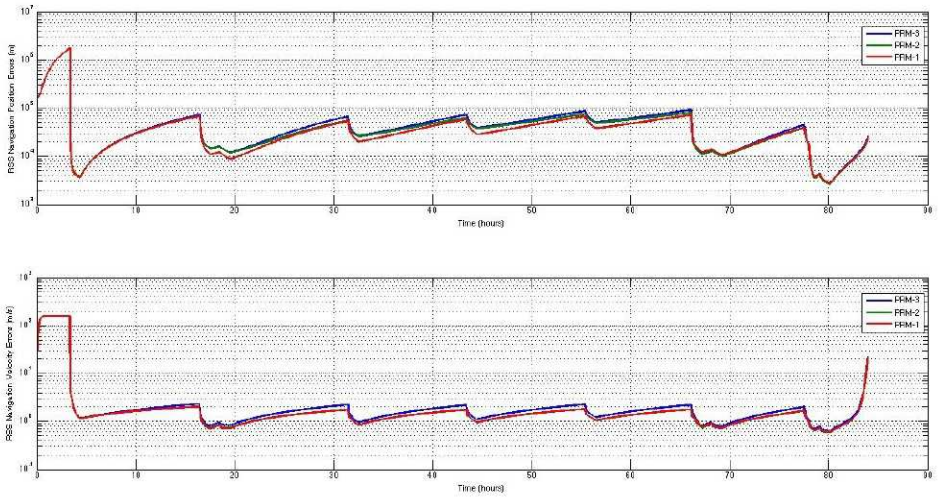

Figure 8: Extended Kalman filter navigation errors for celestial navigation and a variety of state parameterization options.

As with the linearized Kalman filter, the extended Kalman filter shows optimal performance with the PRM-1 state parameterization option. Again, this is due to the relative weakness of the celestial navigation measurements and the weak dynamics of cis-lunar flight.

Next it is desirable to examine whether the linearized or extended Kalman filter provides optimal navigation performance. Figure 9 illustrates the differences between these filter mechanizations.

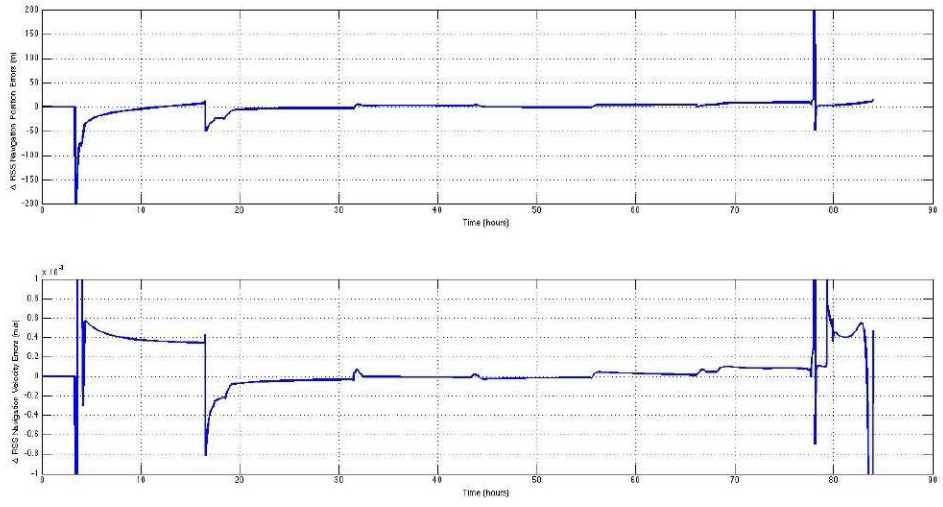

Figure 9: Difference between the linearized Kalman filter and the extended Kalman filter navigation errors.

While very similar in performance, note that there does appear to be a general improvement in performance in the extended Kalman filter as opposed to the linearized Kalman filter. Therefore, the extended Kalman filter mechanization with the PRM-1 state parameterization option is selected as the filtering algorithm for celestial navigation based on these results

More than likely, the slight performance enhancement achieved by the extended Kalman filter over the linearized Kalman filter is due to a reduction in the linearization in filtering algorithms. Instead of using a reference trajectory to compute measurement partials and propagating an error state forward with the state transition matrix, partials are computed with the optimal solution with each time step. Therefore, the affects of non-linear dynamics become minimized. If this assertion is indeed true, one would expect the batch filtering algorithm to have the worst performance.

Sequential Batch Filter Performance for Celestial Navigation

Several state parameterization and batch filtering techniques were examined. The differing batch filtering techniques involved changing the length of each batch size and utilizing different a priori covariances. Table 3 summarizes the various batch filtering techniques studied.

Table 3: Summary of batch filtering techniques examined.

Option	Position Covariance	Velocity Covariance	Batch Length
COV-1	Navigation propagated	Navigation propagated	60 minutes
COV-2	Navigation propagated	Navigation propagated	30 minutes
COV-3	100 km each axis	10 m/s each axis	60 minutes
COV-4	Canned covariance schedule	Canned covariance schedule	60 minutes
COV-5	None	None	60 minutes

For COV-1 and COV-2, the navigation computed covariance was propagated to the start of each new measurement pass and utilized as the initial covariance. COV-3 utilized the same spherical inertial covariance as the a priori covariance. COV-4 attempted to optimize the use of a canned covariance only at certain events (sphere of influence crossings and post TCMs). The schedule for the COV-4 is shown in Table 4. The COV-5 configuration utilized no a priori covariance information.

Table 4: COV-4 covariance schedule.

Option	Position Covariance	Velocity Covariance	Batch Length
First optical nav	10 km each axis	10 m/s each axis	60 minutes

pass			
Sphere of influence crossing	10 km each axis	10 m/s each axis	60 minutes
Post TCM-5	10 km each axis	10 m/s each axis	60 minutes
Day 2 optical nav pas	Navigation propagated	Navigation propagated	60 minutes
Day 2 optical nav second pass	Navigation propagated	Navigation propagated	60 minutes
Day 3 optical nav pass	Navigation propagated	Navigation propagated	60 minutes
Pre TCM-6 pass	Navigation propagated	Navigation propagated	60 minutes
Post TCM-6 pass	10 km each axis	10 m/s each axis	60 minutes
Pre TCM-7 pass	Navigation propagated	Navigation propagated	60 minutes
Post TCM-7 pass	10 km each axis	10 m/s each axis	60 minutes

Clearly, there are many more potential batch filtering configurations possible, such as geometrically skewing the initial covariance and further adjustments of the batch length. Many of these configurations were tried for this study, but for the sake of brevity are not shown. The sample documented in this paper was chosen as reflective of the batch filtering performance.

First, the PRM-3 state parameterization configuration was tried for the detailed COV configurations. Figure 10 illustrates the navigation performance for this state parameterization option, with the extended Kalman filter performance included for comparison.

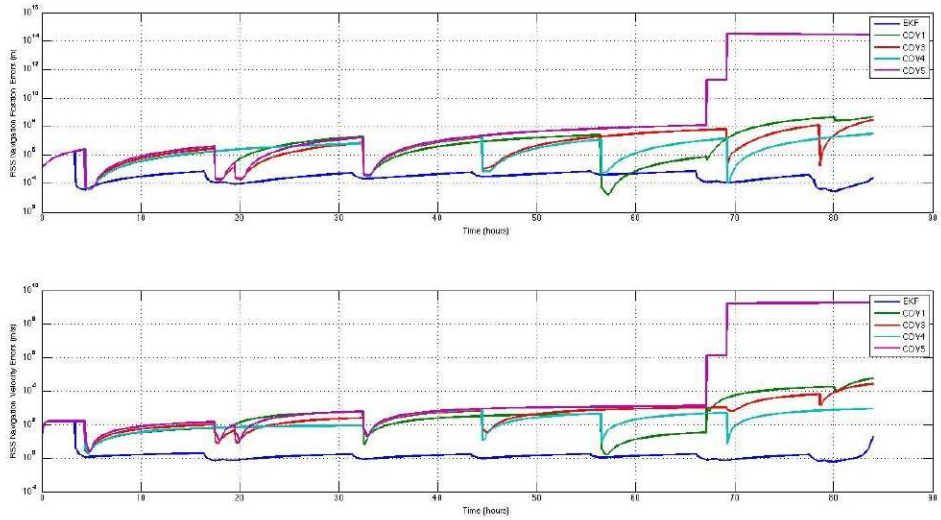

Figure 10: Navigation errors for PRM-3 and batch filtering for a variety of COV configurations.

Note that COV-2 was not illustrated as the batch filter computed a matrix that was not positive definite and could not be inverted (ie, the filter became unstable). Additionally, the COV-5 option seemed to indicated a diverging filter. Note how in all cases, the extended Kalman filter mechanization out-performs the sequential batch filter.

Next, the same COV configurations were examined for the PRM-2 state parameterization.

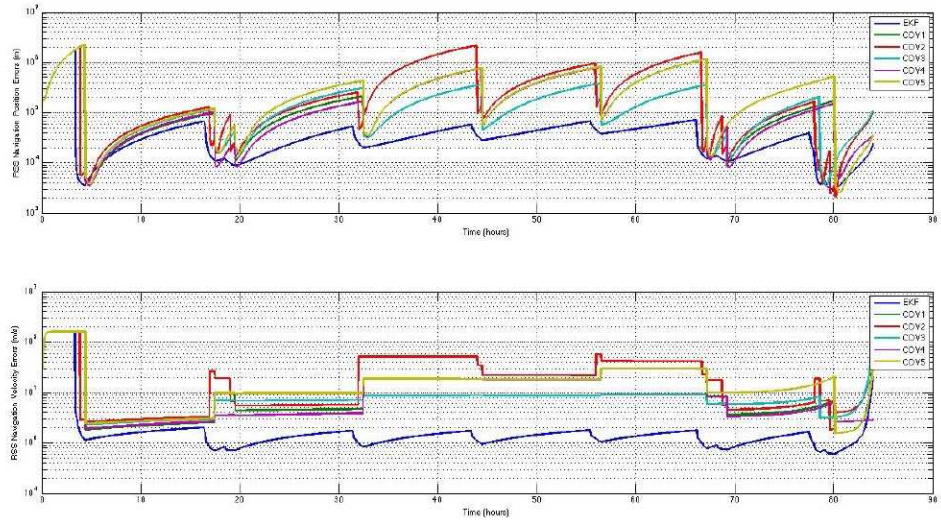

Figure 11: Navigation errors for PRM-2 state parameterization and batch filtering

for a variety of COV configurations.

Again, it is shown the extended Kalman filter outperforms the sequential batch filter. Finally, the PRM-1 state parameterization is examined. The performance of this parameterization option is illustrated in Figure 12.

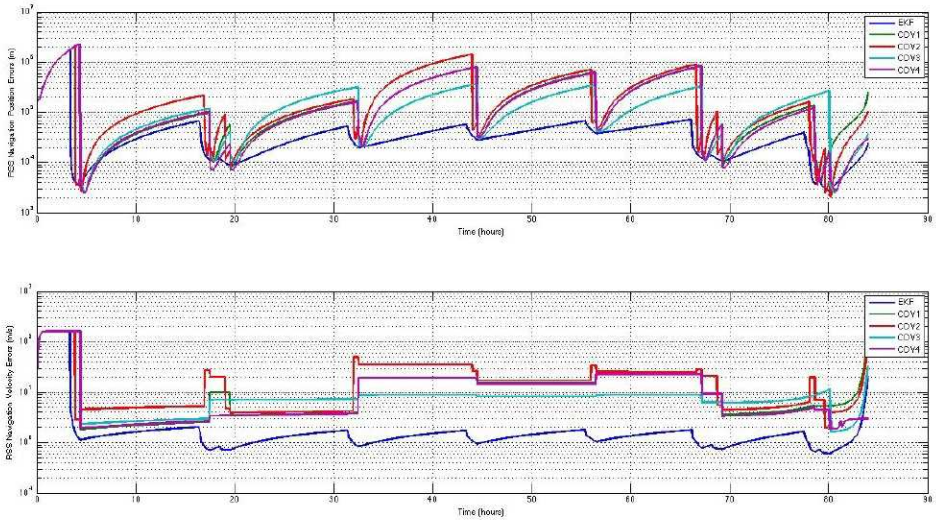

Figure 12: Navigation errors for PRM-1 state parameterization and a variety of COV configurations.

Note for the COV-5 option, the batch filter again computed normal matrices that did not stay positive definite. Also note that again the extended Kalman filter outperforms the sequential batch filter.

Clearly, the extended Kalman filter is shown to provide superior navigation performance to many manifestations of the sequential batch filtering algorithm for optical navigation. This, coupled with noting that often times the batch filter appears to diverge in cis-lunar space, confirms the previous assertion that the additional linearization involved in the batch filtering algorithm is not suitable for celestial navigation.

Extended Kalman Filter Performance for Lunar Landmark Tracking

Recall that simplicity of use and consistency between celestial navigation and lunar landmark tracking was to be considered in making the selection of the optical navigation filter design. Since it has already been shown that an extended Kalman filter with the PRM-1 state parameterization is the optimal algorithm for celestial navigation, the same trade space does not need to be performed for lunar landmark tracking. All that is necessary, is to show that the extended Kalman filter with PRM-1 state parameterization is sufficient for lunar landmark tracking operations. Figure 13 illustrates the navigation

performance for lunar landmark tracking for a 100 km orbit about the Moon. In the next section, a more detailed examination of the ability of optical navigation to meet specific performance requirements will be made.

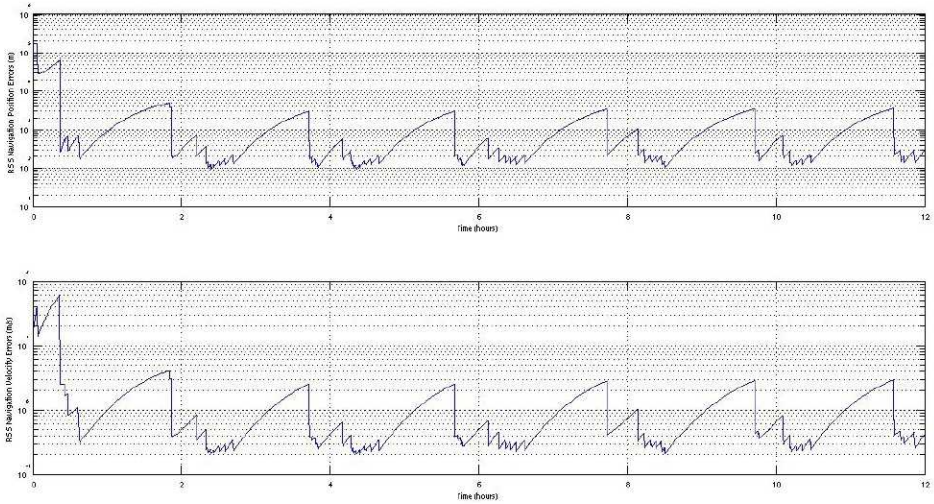

Figure 13: Lunar landmark navigation performance with PRM-1 state parameterization and extended Kalman filter.

OPTICAL NAVIGATION PERFORMANCE VS. REQUIREMENTS

Assessment of Δv Dispersions

Orion is required to constrain the Δv dispersions for the TEI sequence and the TCMs to within 20 m/s. As part of the design evaluation of the magnitude of Δv dispersions, the Orion program has developed error budgets and the corresponding partials for various contributors to Δv dispersions (e.g., navigation, control, propellant system, etc.)[2]. For radiometric navigation, the design evaluation yielded a 3σ Δv dispersion well within the budgeted 20 m/s. Utilizing the partials developed to assess the navigation sensitivity, it can be estimated that the optical navigation design will yield an adequate 3σ Δv dispersion

Entry Interface Conditions

The second relevant requirement concerns the ability to hit the entry interface conditions. For a nominal return, the Orion vehicle will use a skip entry profile in order to bleed off energy to obtain a precision landing off the coast of San Clemente, California. For the skip entry, the driving entry interface condition is the entry flight path angle which is required to be 0.12°, 3σ. The ability to achieve this tight requirement is primarily driven

by navigation performance. Table 5 lists the ability of both nominal radiometric navigation and celestial navigation to resolve the entry flight path angle.

Table 5: Ability of cis-lunar navigation to achieve entry flight path angle.

Navigation Method	3σ Flight Path Angle
Radiometric Navigation	0.1°
Celestial Navigation	0.5°

Celestial navigation will not achieve the entry flight path angle with sufficient fidelity to perform skip entry operations. Orion has two entry downmodes: 1) Loads-managed guided entry and 2) ballistic type entry , both of which can be performed with flight path angle dispersions on the order of 1°, 3σ. This means while precision landing off the coast of San Clemente cannot be achieved, celestial navigation is capable of returning a crew safely to Earth.

SUMMARY & CONCLUSIONS

The Orion optical navigation system is design to enable a safe crew return to Earth in the event of loss of communications with the vehicle. Such operations will sacrifice the precision landing off the coast of San Clemente as the required entry interface conditions for the precision landing would be difficult to meet for this contingency scenario.

Previous work has focused on the feasibility of optical navigation and expected performance of optical navigation. The work presented in this paper takes the Orion optical navigation a step further and examines various filtering mechanisms as well as state parameterization options. It has been shown that weak dynamics in the cis-lunar phase of flight coupled with weak measurement observability limit the ability to solve for measurement biases. Additionally it has been shown that algorithms with a high dependence on linearization (sequential batch and linearized Kalman filter) have degraded performance with respect to an extended Kalman filter. Furthermore, the extended Kalman filter has been shown to meet Orion requirements with respect to Δv dispersions and entry interface conditions.

FUTURE WORK

The camera characteristics for Celestial Navigation and Lunar Landmark Tracking are currently being determined. Based on those characteristics, a trade study will be performed and a recommendation will be made to use either one of several existing cameras: star trackers, centerline docking camera, situational awareness cameras or a separate, stand-alone camera for the specific purpose of optical navigation. Completion of the following steps will establish the baseline for the Orion optical navigation system:

1. Assess Lunar photometric characteristics based on an assumed phase function and Lambertian reflectance
2. Finalize measurement error budgets for lunar landmark and star-horizon measurements for their allocations to support optical navigation state accuracy
3. Assess optical navigation state prediction capability needed to support landmark acquisition
4. Define the camera characteristics needed to support landmark tracking, star-horizon measurements and apparent diameter measurements
5. Perform trade to select from existing hardware or propose new block upgrade option
6. Revisit ConOps for loss of communication scenario to determine when each measurement type will be acquired
7. Construct landmark tracking catalog based on measurement error allocation
8. Develop the image processing algorithms for Celestial Navigation and Lunar Landmark Tracking measurements
9. Assess optical navigation system performance

REFERENCES

1. Clark, Fred, "Candidate Stars for Celestial Navigation", NASA Internal Report, FltDyn-CEV-06-118, 2006.
2. Crain, Timothy, "Orbit Mode Team Error Budgets", NASA Internal Report, 2009.
3. Gelb, Arthur, "Applied Optimal Estimation", The Analytical Sciences Corporation, 1974.
4. Getchius, Joel, Crain, T., and D'Souza, C., "Optical Navigation for the Orion Vehicle" *AAS/AIAA Space Flight Mechanics Meeting,* AAS 08-105, San Luis Resort, TX, January 20008.
5. Getchius, Joel, Kubitschek, Daniel, and Crain, Timothy., "Orion Navigation Sensitivities to Ground Station Infrastructure for Lunar Missions" *AAS Guidance and Control Conference*, AAS 08-056, Beaver Run Resort, CO, February 2008.
6. Hanak, F. Chad, "Lost in Low Lunar Orbit Crater Pattern Detection and Identification," PhD Dissertation, University of Texas at Austin, Department of Aerospace Engineering and Engineering Mechanics, May 2009.
7. "Planetary Interactive G.I.S.-on-the-Web Analyzable Database," US Geological Survey Planetary GIS Web Server, *webgis.wr.usgs.gov/index.html*.
8. Osenar, Michael, "Performance of Automated Feature Tracking Cameras for Lunar Navigation," *Rice University*, 2007.
9. Zanetti, Renato, "Autonomous Mid-Course Navigation for Lunar Return", NASA Internal Report, FltyDyn-CEV-08-139, 2008.